Mahidol University Faculty of Environment and Resource Studies
ENVI MAHIDOL ENRIC
The 6th Environment and Natural Resources International Conference (ENRIC 2026)
Theme: Real World Impact: Resilience for a Changing Climate
24 - 25 November 2026, Bangkok, Thailand

Assessment of $PM_{2.5}$ Exposure and Health Risks in Chiang Mai, Thailand: Mapping Spatial Risk Clusters Using Remote Sensing and GIS

Worawit Suppawimut*, Phonpat Hemwan , Watinee Thavorntam , and Arisara Charoenpanyanet

Department of Geography, Faculty of Social Sciences, Chiang Mai University, Chiang Mai 50300, Thailand
**Corresponding Author E-mail: worawit_sup@cmu.ac.th*

ABSTRACT

Fine particulate matter ($PM_{2.5}$) is a major public health threat in Chiang Mai, Thailand. This study examined the spatial distribution of $PM_{2.5}$ health risk during the peak burning period (January–April) from 2020 to 2024 by integrating remote sensing and GIS in a multidimensional framework (Risk = Hazard × Exposure × Vulnerability). Hazard was represented by Satellite-derived $PM_{2.5}$, exposure by population density, and vulnerability indicators by historical burn probability and proximity to healthcare facilities. Spatial clustering was detected using Global and Local Moran's I, and school locations were assessed for potential impacts on sensitive populations.

Significant positive spatial autocorrelation was observed (Moran's I = 0.095, $p < 0.01$). Although 74.24% of the province was classified as low or very low risk, 11.30% was classified as high or very high risk (10.12% and 1.18%, respectively). High-risk areas were concentrated mainly in the central lowland basin and northern border districts. Mueang Chiang Mai had the highest percentage of a very high-risk area in the province at 33.72% followed by Fang, Saraphi, San Kamphaeng, and San Sai, respectively. Furthermore, 80.73% of school locations fell within high- or very-high-risk zones. Local Moran's I further identified statistically significant High–High clusters primarily in the central and northern areas. These findings reveal substantial spatial variation in $PM_{2.5}$-related health risk driven by the combined effects of hazard, population exposure, and vulnerability. The results provide a spatial basis for targeted air pollution preparedness and risk-reduction planning during the burning season.

Keywords: $PM_{2.5}$ Exposure/ Spatial Risk Assessment / Spatial Vulnerability / GIS

1. INTRODUCTION

Air pollution is a major threat to global public health, contributing substantially to morbidity and mortality. According to the World Health Organization (WHO), 99% of the global population is exposed to air containing unhealthy levels of fine particulate matter ($PM_{2.5}$). In 2023, the global mean annual $PM_{2.5}$ concentration was 26 μg/m³, more than five times the WHO guideline of 5 μg/m³ [1]. $PM_{2.5}$ is strongly associated with adverse health outcomes, including cardiovascular disease, lung cancer, asthma, and chronic obstructive pulmonary disease (COPD). In Northern Thailand, particularly Chiang Mai Province, severe $PM_{2.5}$ episodes recur annually during the dry season due to agricultural burning, forest fires, and transboundary haze [2–3]. The mountainous terrain surrounding the Chiang Mai basin can restrict atmospheric dispersion and contribute to pollutant accumulation, while the province's proximity to international borders increases the potential influence of regional pollution sources [4–6].

Previous studies in Thailand have reported associations between $PM_{2.5}$ exposure and adverse health outcomes, including respiratory disease, hospital admissions, and premature mortality [8–10]. In upper northern Thailand, seasonal haze periods are significantly associated with acute health crises, particularly increased COPD fatality and hospital re-admission rates following short-term exposure to elevated $PM_{2.5}$ concentrations [9]. Furthermore, quantitative health risk assessments indocate the severe long-term impacts, with ambient $PM_{2.5}$ accounting for approximately 30.5% of cardiopulmonary and 41.8% of lung cancer mortality risks among the adults [10]. However, assessment based primarily on pollutant concentration or population exposure does not fully capture the spatial dimension of risk.

Populations exposed to similar $PM_{2.5}$ concentrations may experience different levels of risk because of differences in population distribution, environmental conditions, and access to essential services.

A spatial risk perspective is particularly relevant where $PM_{2.5}$ concentrations, population exposure, and vulnerability vary across space. Previous studies have demonstrated the value of integrating remote sensing and Geographic Information Systems (GIS) for $PM_{2.5}$ exposure and health-risk assessment. Xu et al. [11] combined satellite-derived $PM_{2.5}$, population density, and GIS at a 1-km grid to assess exposure risk in the Shanghai–Hangzhou Bay region, identifying higher risks in densely populated areas. Song et al. [12] evaluated regional and population exposure risks across China using satellite-derived $PM_{2.5}$ and population-weighted measures, revealing clear spatial and seasonal variations in exposure risk. In Thailand, Tabucanon et al. [13] applied GIS-based risk mapping in Bangkok, integrating $PM_{2.5}$ concentrations, population distribution, and vulnerability indicators to support local risk-reduction planning. These studies demonstrate the value of spatial approaches for identifying concentrated $PM_{2.5}$ risks; however, assessments that jointly integrate $PM_{2.5}$ hazard, population exposure, vulnerability, and local spatial clustering across heterogeneous provincial landscapes remain limited in Northern Thailand.

To address this gap, this study assesses the spatial distribution and clustering of $PM_{2.5}$-related health risks in Chiang Mai Province using a multidimensional risk framework, expressed as Risk = Hazard × Exposure × Vulnerability. Satellite-derived $PM_{2.5}$ concentrations were used to represent the hazard, population density to characterize exposure, and selected vulnerability-related indicators to represent differences in environmental susceptibility and coping capacity. GIS-based spatial analysis was used to produce a composite risk surface, while Global Moran's I and Local Moran's I (LISA) were applied to examine overall spatial dependence and identify significant risk clusters. The study further examines the distribution of educational institutions within risk zones to highlight potential implications for sensitive populations. The resulting spatial evidence is intended to support geographically targeted $PM_{2.5}$ preparedness and risk-reduction planning in areas where health risks are concentrated.

2. METHODOLOGY

2.1 Study area

The study area encompasses Chiang Mai Province in Northern Thailand (17°14′–20°08′ N, 98°00′–99°34′ E), covering an area of approximately 20,107 km^2. The province shares a northern international border with Myanmar to the north and is bordered by Chiang Rai to the northeast, Lamphun to the south, and Mae Hong Son to the west. Chiang Mai comprises 25 districts (Fig. 1) and had a population of 1.79 million in 2024, with approximately 220,000 residents concentrated in Mueang District.

The province is characterized by mountainous terrain surrounding central lowlands, forming a basin-like landscape that restricts atmospheric ventilation and promotes pollutant accumulation. The mean annual temperature is 25.4°C, ranging from 20.1°C to 31.8°C. According to the Pollution Control Department [14], the 2024 annual mean $PM_{2.5}$ concentration at monitoring station 35T in Suthep Subdistrict was 30 µg/m^3, with a maximum of 156.5 µg/m^3 and 77 days exceeding the 24-hour national standard of 37.5 µg/m^3.

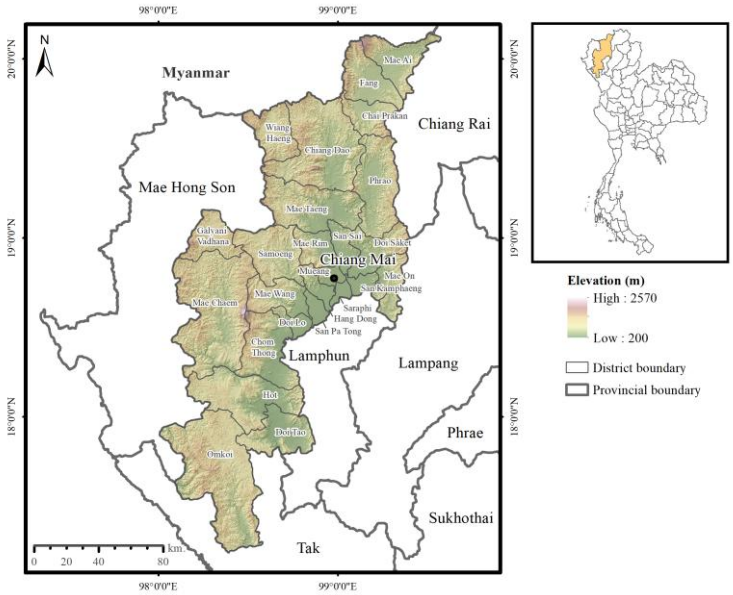

Figure 1. Map of Chiang Mai Province

2.2 $PM_{2.5}$ Risk Assessment

This study adopted a multidimensional spatial risk assessment framework to evaluate the impact of $PM_{2.5}$ pollution. The spatial health risk was conceptualized as a function of three interconnected domains: Hazard (H), Exposure (E), and Vulnerability (V). The relationship is expressed as:

$$Risk = Hazard \times Exposure \times Vulnerability \quad (1)$$

2.2.1 $PM_{2.5}$ Hazard

The hazard component (H) was derived from satellite-estimated $PM_{2.5}$ concentration data. To capture the persistent spatial patterns of air pollution, a five-year average (2020–2024) from a previous phase of this research, which estimated ground-level $PM_{2.5}$ using AOD and Sentinel-5P observations [7], was calculated for the severe smoke haze season (January to April). The derived gridded $PM_{2.5}$ estimates were utilized for analysis with population density data in the following step (Fig. 2).

2.2.2 Relative Population Exposure Risk

The public health risk of $PM_{2.5}$ is influenced by population distribution (Fig. 2). To quantify this demographic exposure, a relative risk model was applied [11-12] by integrating the $PM_{2.5}$ hazard layer with high-resolution population density data [15]. Rather than estimating an absolute epidemiological burden, this approach normalizes exposure across the provincial domain. This comparative framework highlights extreme risk zones where severe air pollution coincides with human settlements. The relative exposure was calculated as:

$$\boldsymbol{RER_i = \frac{P_i \times H_i}{\frac{1}{n}\sum_{i=1}^{n}(P_i \times H_i)}} \quad (2)$$

where RER_i is the relative population exposure risk in grid i; P_i is the population density (persons/km^2) of grid i; H_i is the five-year average $PM_{2.5}$ concentration (μg/m^3) of grid i during the burning period; and n is the total number of grids within the study area.

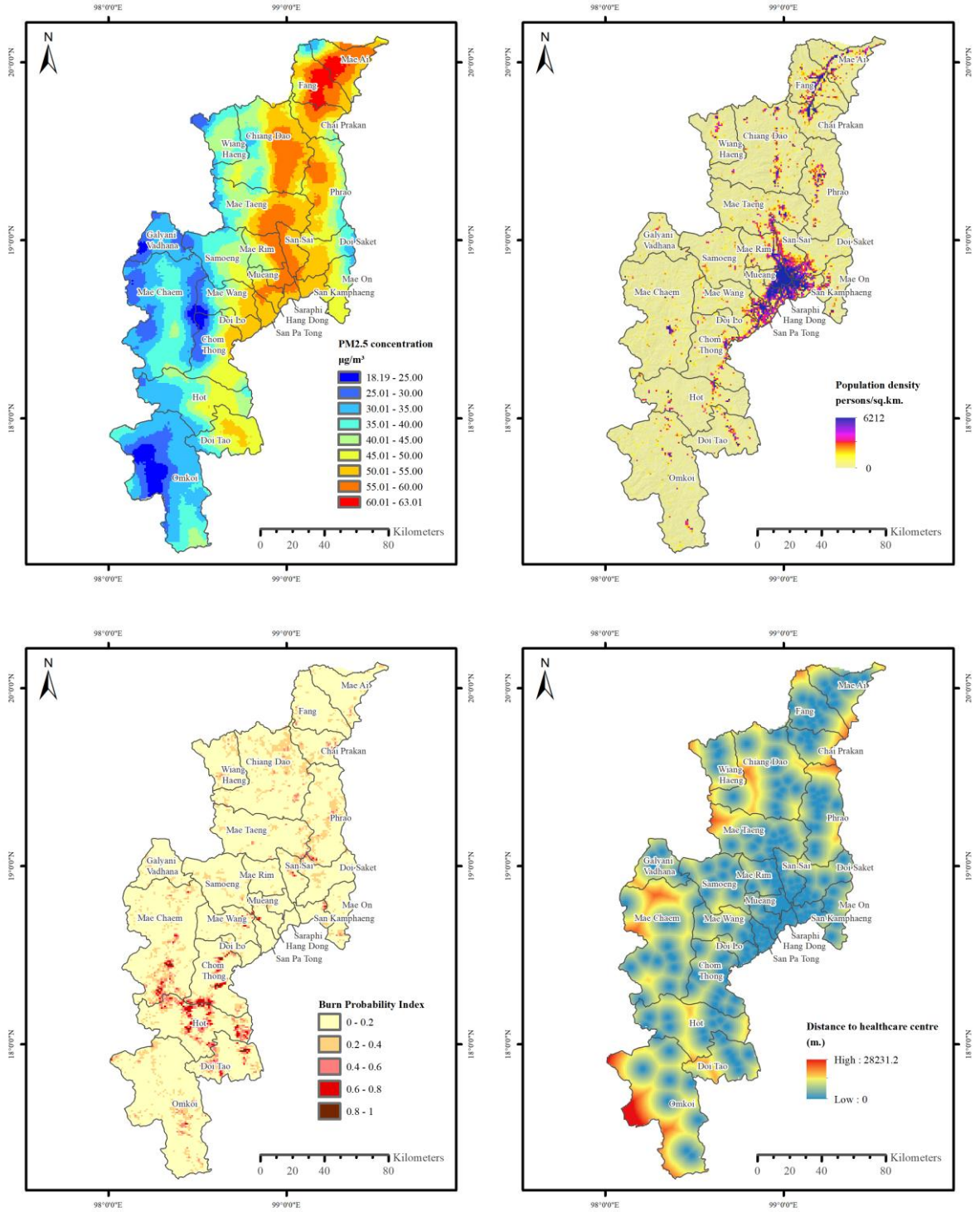

Figure 2. Spatial criteria maps utilized for the $PM_{2.5}$ risk assessment model in Chiang Mai Province, showing the $PM_{2.5}$ hazard (upper left), population density (upper right), burn probability (bottom left), and distance to healthcare centres (bottom right).

2.2.3 Spatial Vulnerability Assessment

To assess vulnerability (V), two components were considered: historical burn probability representing environmental susceptibility, and proximity to healthcare facilities representing limited infrastructural access and coping capacity (Fig. 2). This approach captures both the likelihood of localized emissions and differences in access to healthcare services.

Environmental Vulnerability (V_1): Historical burn probability was used to represent environmental susceptibility, reflecting the likelihood of recurrent biomass burning impacts. The MODIS Burned Area product (MCD64A1, Collection 061) [16] was processed in Google Earth Engine (GEE) for the smoke haze season (January to April) from 2020 to 2024. Monthly data were converted to binary burn masks and aggregated to calculate cumulative burn frequency per 1 km spatial unit. Dividing by the five year period yields a historical burn probability index ranging from 0.0 (no historical fires) to 1.0 (burned annually), identifying area prone to recurrent biomass burning (Fig. 2).

Infrastructural Vulnerability (V_2): Distance to healthcare facilities represents limited healthcare access and reduced coping capacity. Euclidean distance to healthcare facilities was calculated in GIS. Healthcare accessibility may influence air pollution-related health outcomes, as epidemiological evidence indicated that access to emergency medical facilities can reduce $PM_{2.5}$-associated mortality [17]. Incorporating this metric explicitly accounts for disparities in medical intervention capabilities, prioritizing highly vulnerable populations residing in areas with deficient healthcare access.

2.2.4 Risk Integration

All spatial variables representing Hazard, Exposure, and Vulnerability were normalized to a 0–1 scale. The Vulnerability index (V_{norm}) was calculated as the means of the two normalized sub-indicators using equal weights. This approach provides transparent baseline and avoids researcher-defined differential weighting in the absence of locally derived empirical weights. The calculation of the Vulnerability index is expressed as follows:

$$\boldsymbol{V_{norm} = \frac{V_1 + V_2}{2}} \tag{3}$$

The final comprehensive *$PM_{2.5}$ health risk index* (R_{index}) was computed by multiplying the primary risk components, expressed as:

$$\boldsymbol{R_{index} = H_{norm} \times E_{norm} \times V_{norm}} \tag{4}$$

The final risk map was classified into five levels (Very Low, Low, Medium, High, and Very High) using the Geometric Interval classification method. Furthermore, educational institution data were obtained from the Nostra Map database and represented as geographic point features. The analysis evaluates the spatial overlap between school locations and the identified $PM_{2.5}$ risk zones.

2.3 Spatial Autocorrelation and Clustering Analysis

Spatial autocorrelation was applied using GeoDa to evaluate the spatial distribution of comprehensive health risks. The continuous raster risk surface was converted into a polygon format for spatial analysis. A spatial weights matrix was constructed using the first-order Queen contiguity rule.

2.3.1 Global Spatial Autocorrelation

The Univariate Moran's I statistic was calculated to assess the overall spatial autocorrelation and verify whether the $PM_{2.5}$ health risks exhibited a statistically clustered, random, or dispersed pattern across the province.

$$\boldsymbol{I = \frac{\sum_{i=1}^{n}\sum_{j=1}^{n} w_{ij}(x_i - \bar{x})(x_j - \bar{x})}{\frac{1}{n}\sum_{i=1}^{n}(x_i - \bar{x})^2 \sum_{i=1}^{n}\sum_{j=1}^{n} w_{ij}}} \tag{5}$$

where I is the global Moran's I statistic, n is the total number of spatial units, x_i and x_j represent the comprehensive health risk levels (1-5) at locations i and j, $\bar{x}$ is the mean risk level across all spatial

units, and w_{ij} is the spatial relationship between units i and j. The Moran's I index ranges from −1 to 1, with positive values indicate the spatial clustering of similar risk levels (e.g., contiguous high-risk or low-risk zones), negative values indicating a spatial dispersion, and values near zero suggest a random spatial distribution with no spatial autocorrelation.

2.3.2 Local Spatial Autocorrelation

The Univariate Local Moran's I was applied to identify significant local clusters and spatial outliers. This local analysis classified the spatial unit into significant hot spots (High-High clusters), cold spots (Low-Low clusters), and spatial outliers (High-Low and Low-High), providing a robust foundation for spatially targeted mitigation strategies.

$$I_i = \frac{(x_i - \bar{x})}{S^2} \sum_{j=1}^{n} w_{ij}(x_j - \bar{x}) \quad (6)$$

$$S^2 = \frac{1}{n} \sum_{i=1}^{n} (x_i - \bar{x})^2 \quad (7)$$

where I_i is the local Moran's I statistic for specific spatial unit i, and S^2 is the variance of the comprehensive health risk levels. The LISA framework classifies High–High (HH) and Low-Low (LL) clusters as hotspots and coldspots, respectively, and High–Low (HL), Low–High (LH) patterns as spatial outliers. These results were utilized to identify the geographical boundaries of critical $PM_{2.5}$ health risk zones across the study area.

3. RESULTS AND DISCUSSION

3.1 $PM_{2.5}$ Risk Map

The spatial distribution of seasonal $PM_{2.5}$ health risks across Chiang Mai Province shows a distinct spatial pattern, with higher-risk areas concentrated in the central basin and northern districts. Overall, 1.18% (258 km^2) of the provincial area was classified as Very High risk, 10.12% (2,203 km^2) as high risk, and 14.46% (3,148 km^2) as medium risk. Figure 3 shows that Very-high-risk zones were primarily concentrated in the urban core, particularly Mueang Chiang Mai, and extended into adjacent districts, including Saraphi, San Kamphaeng, and San Sai. A second cluster of Very High risk was identified in the northern districts of Fang and Mae Ai. High risk areas formed a broader corridor across the central valley, including Mae Rim, Mae Taeng, and Chiang Dao. In contrast, the western and southern mountainous districts, particularly Mae Chaem, Galyani Vadhana, and Omkoi, were predominantly classified as Low risk or Very low risk with isolated High-risk areas mainly concentrated around their urban communities and district centers.

The highest-risk areas are concentrated in a limited number of districts. Mueang Chiang Mai contained the largest Very high risk area, covering 87 km^2 and accounting for 33.72% of the total very high-risk area (Fig. 4). Fang and Saraphi each account for 21 km^2 (8.14%), followed by San Kamphaeng with 19 km^2 (7.36%) (Table 1). The High risk category covered a broader area across northern and surrounding districts. Fang had the largest High risk area (169 km^2; 7.67%), followed by Chiang Dao (168 km^2; 7.63%) and Mae Taeng (149 km^2; 6.76%). Overall, the most severe $PM_{2.5}$ risks were concentrated in densely populated areas of the central basin, while broader High-risk zones extended across the northern districts. This spatial pattern is consistent with previous studies showing that $PM_{2.5}$ exposure risks tend to increase where elevated pollution levels overlap with greater population exposure [11,12].

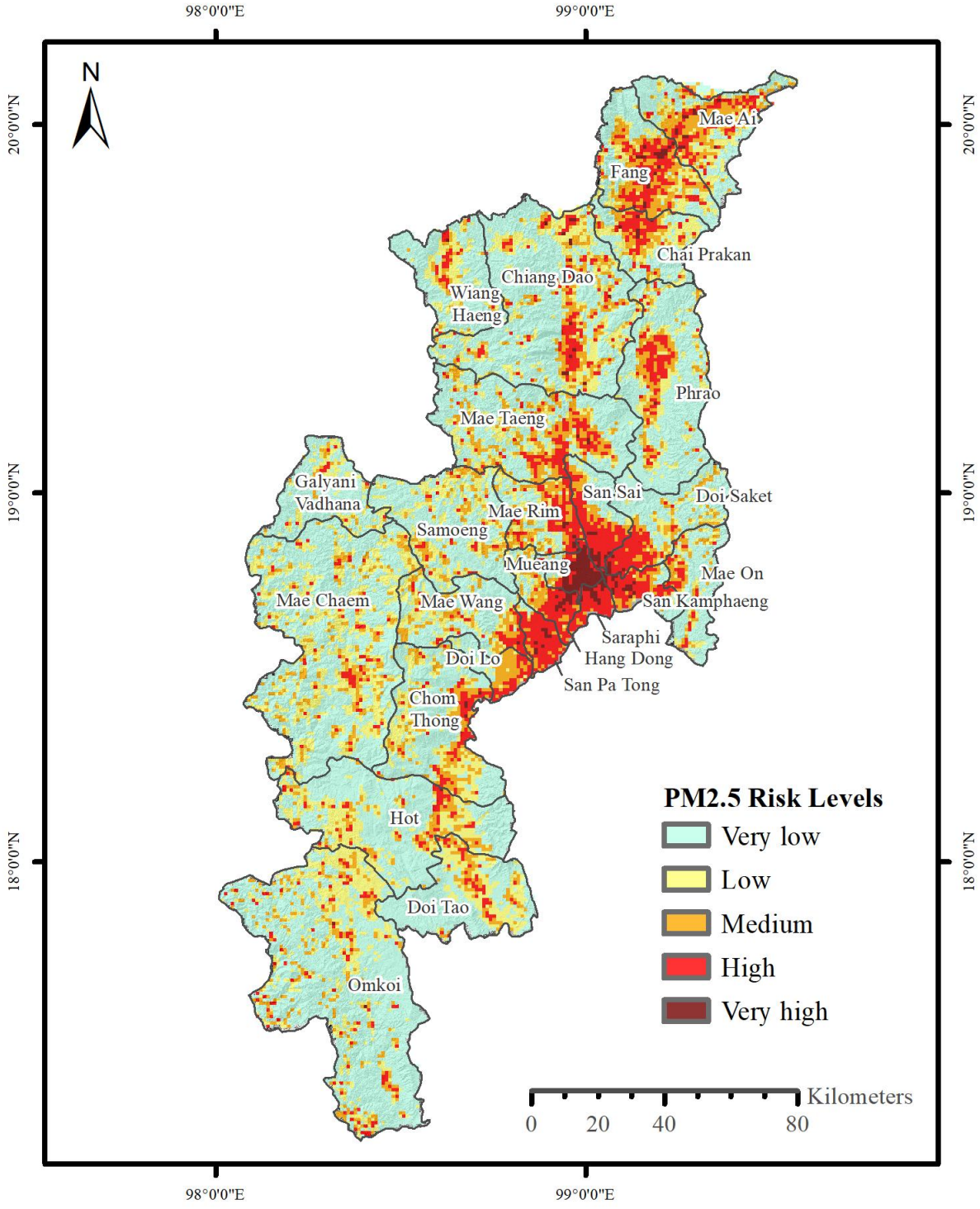

Figure 3. Map of $PM_{2.5}$ Risk in Chiang Mai

Table 1. District-level classification of $PM_{2.5}$ spatial risk zones during the peak haze season in Chiang Mai Province.

District name	Very High		High		Medium		Low		Very Low	
	Sq.km.	%	Sq.km.	%	Sq.km.	%	Sq.km.	%	Sq.km.	%
Mueang Chiang Mai	87	33.72	41	1.86	14	0.44	10	0.23	32	0.27
Fang	21	8.14	169	7.67	222	7.05	131	3.00	251	2.13
Saraphi	21	8.14	72	3.27	7	0.22	0	0.00	0	0.00
San Kamphaeng	19	7.36	92	4.18	46	1.46	11	0.25	55	0.47
San Sai	18	6.98	137	6.22	59	1.87	17	0.39	110	0.93
Mae Ai	17	6.59	120	5.45	213	6.77	151	3.46	274	2.32
Hang Dong	17	6.59	84	3.81	70	2.22	48	1.10	44	0.37
Chiang Doa	14	5.43	168	7.63	265	8.42	435	9.96	1,293	10.96
San Pa Tong	9	3.49	123	5.58	25	0.79	5	0.11	8	0.07
Doi Saket	9	3.49	112	5.08	99	3.14	70	1.60	356	3.02
Mae Rim	7	2.71	122	5.54	127	4.03	87	1.99	112	0.95
Chai Prakan	6	2.33	87	3.95	95	3.02	131	3.00	196	1.66
Chomthong	4	1.55	87	3.95	198	6.29	249	5.70	565	4.79
Mae Taeng	3	1.16	149	6.76	292	9.28	212	4.85	746	6.32
Omko	2	0.78	104	4.72	254	8.07	537	12.29	1,860	15.77
Phrao	1	0.39	113	5.13	153	4.86	180	4.12	829	7.03
Wiang Haeng	1	0.39	38	1.72	49	1.56	152	3.48	440	3.73
Hot	1	0.39	72	3.27	154	4.89	328	7.51	920	7.80
Mae Wang	1	0.39	57	2.59	121	3.84	176	4.03	324	2.75
Mae Chaem	0	0.00	74	3.36	280	8.89	746	17.07	1,593	13.50
Samoeng	0	0.00	38	1.72	116	3.68	261	5.97	574	4.87
Doi Tao	0	0.00	47	2.13	99	3.14	205	4.69	483	4.09
Mae On	0	0.00	39	1.77	77	2.45	66	1.51	268	2.27
Doi Lo	0	0.00	44	2.00	69	2.19	22	0.50	75	0.64
Galyani Vadhana	0	0.00	14	0.64	44	1.40	139	3.18	390	3.31
All	258	100.00	2,203	100.00	3,148	100.00	4,369	100.00	11,798	100.00

An intra-district analysis further highlights the concentration of $PM_{2.5}$ risks relative to the total area of each district. Mueang Chiang Mai had the highest proportion of Very High risk area, with 47.28% of its total area classified as Very High risk (Fig. 5), followed by Saraphi at 21.00% of its area. The High risk category also dominated several central districts, with 72.35% of San Pa Tong and 72.00% of Saraphi classified as High risk. When Very High and High risk zones were combined, Saraphi (93.00%), San Pa Tong (77.64%), and Mueang Chiang Mai (69.56%) had the largest proportions of their area within these two risk categories, leaving limit area of low-risk zones for their populations.

Furthermore, educational institution locations were overlaid onto the spatial risk map. The analysis revealed that 21.77% of schools are situated in Very High risk areas and 58.96% in High risk areas, cumulatively accounting for 80.73%. Consequently, it is strongly recommended that schools establish designated safe zones equipped with air filtration systems. Additionally, outdoor activities should be strictly limited when pollution levels exceed the 24 hour average standard of 37.5 $\mu g/m^3$. The installation of air quality sensors within school premises is also advised to support local monitoring.

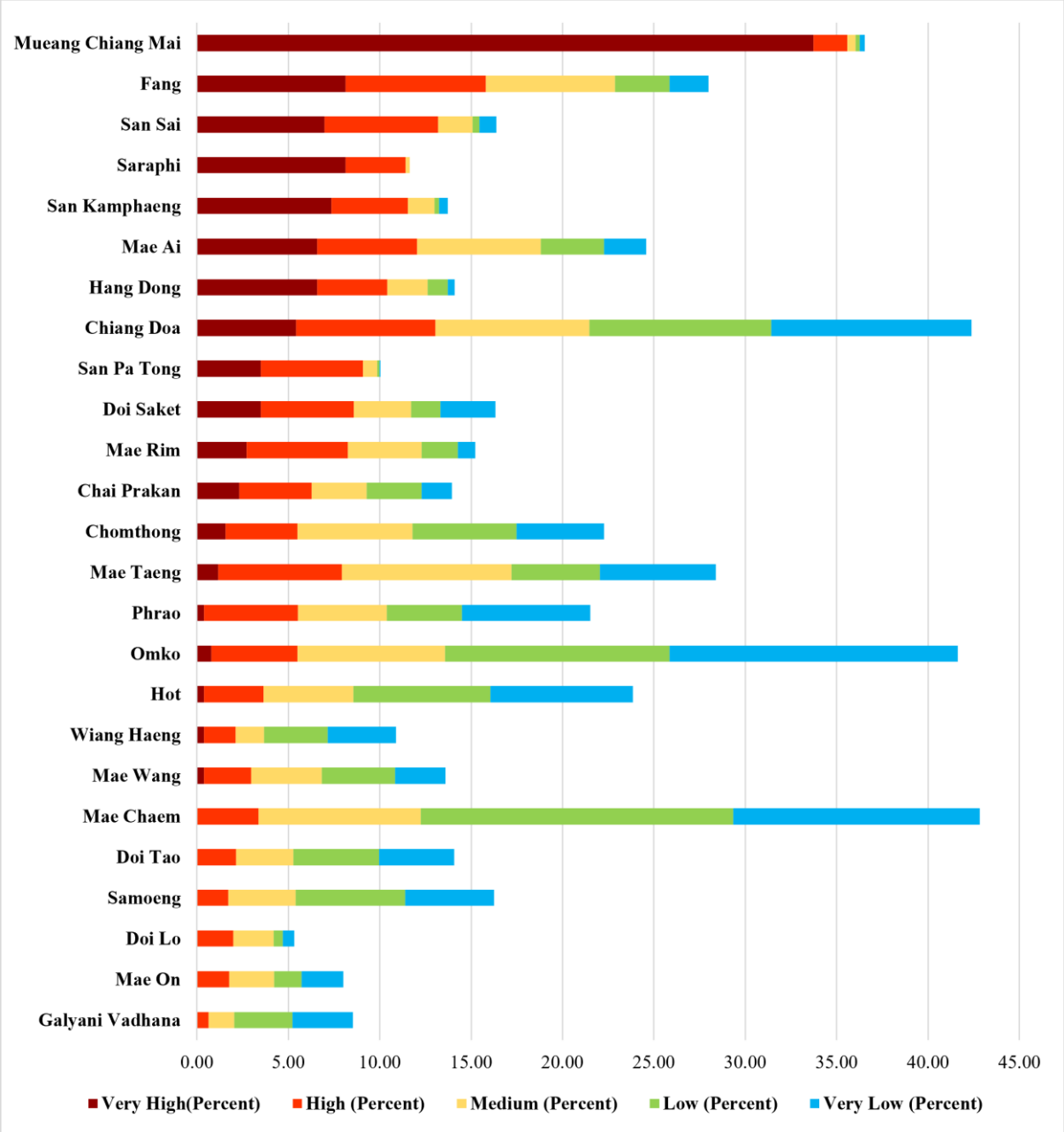

Figure 4. District percentage contribution to the total $PM_{2.5}$ Risk Areas in Chiang Mai

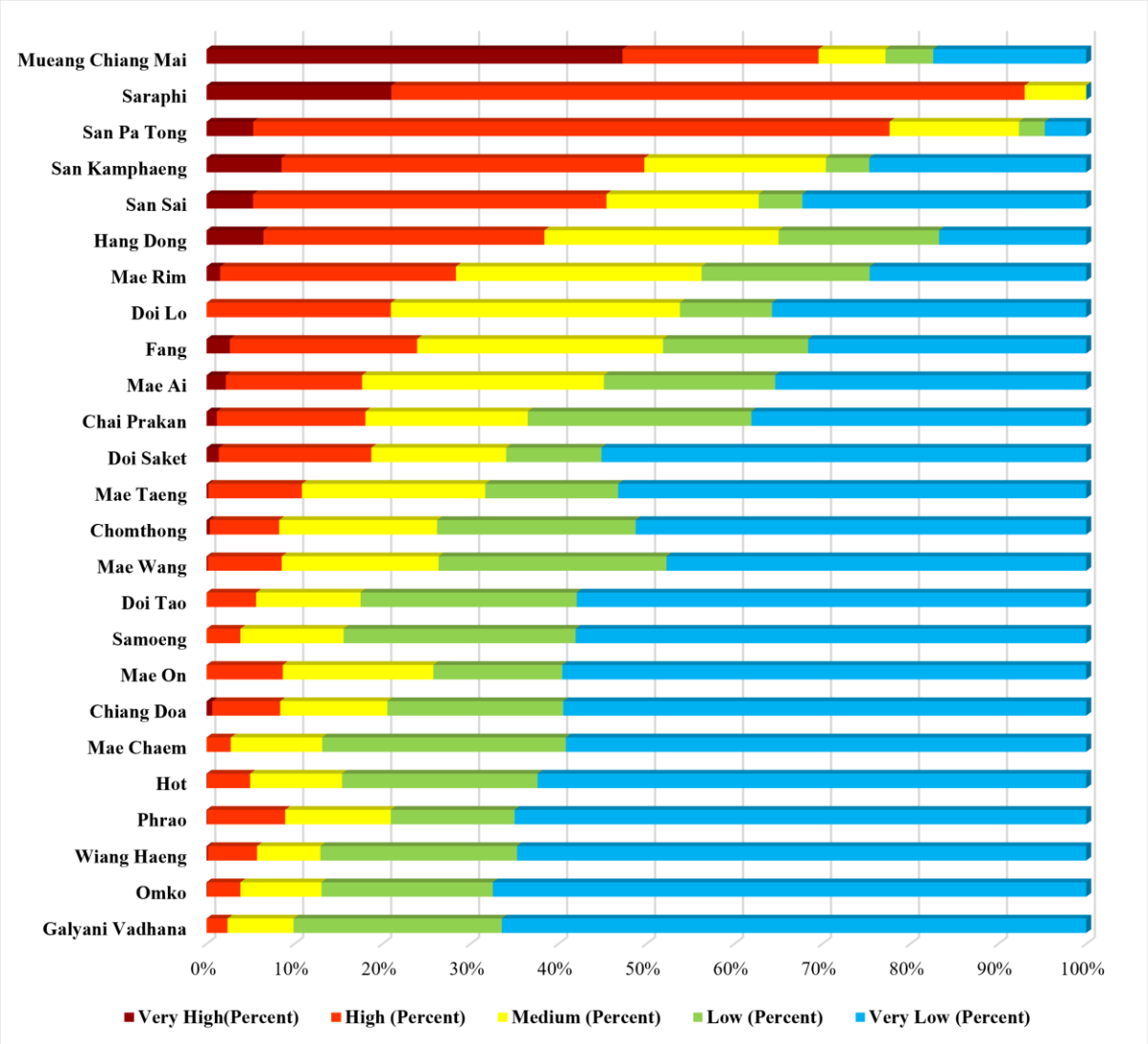

Figure 5. Percentage of $PM_{2.5}$ Risk Levels Within Each District

3.2 Spatial Clustering Analysis of $PM_{2.5}$ Health Risks

The global spatial autocorrelation analysis indicated that comprehensive $PM_{2.5}$ health risks in Chiang Mai Province was significantly spatially clustered rather than randomly distributed. The positive Moran's I value of 0.095 indicates a weak, statistically significant positive spatial autocorrelation (z-score = 8.7378, pseudo p-value = 0.001). This suggests the presence of localized spatial clustering despite a relatively modest overall spatial dependence, supporting further investigation using local spatial autocorrelation analysis.

The Local Moran's I (LISA) analysis further delineated the spatial distribution of significant risk clusters and outliers. A total of 100 grid cells were classified as High–High clusters, indicating localized risk hotspots (Fig. 6). Cross-referencing these clusters with the primary input variables reveals a strong spatial convergence of severe $PM_{2.5}$ hazard and dense human settlement. Geographically, these hotspots are intensely concentrated in the urbanized central basin specifically Mueang, San Sai, Saraphi, Hang Dong, San Pa Tong, and Mae Rim districts. Another hotspot is observed in the northern region near the Thai-Myanmar border, which includes Fang, Chai Prakan, and Mae Ai districts, driven by high atmospheric pollutant accumulation combined with dense local populations.

In contrast, 132 grid cells were identified as Low–Low clusters, mainly in sparsely populated areas with relatively lower $PM_{2.5}$ concentrations. These cold spots are located across the western and

southern mountainous districts, including Mae Chaem, Galyani Vadhana, Samoeng, Hot, Doi Tao, and Omkoi (Fig. 6).

Spatial outliers comprised 587 High–Low and 46 Low–High spatial units, indicating spatial transitions between populated valleys and sparsely populated high altitude area. Local Moran's I identified significant spatial patterns at significance levels at $p \leq 0.05$ and $p \leq 0.001$, while the most of the study area (2,660 spatial units) showed no statistically significant local spatial autocorrelation. These findings reveal substantial spatial heterogeneity in $PM_{2.5}$ health risks across Chiang Mai Province, with statistically significant clusters concentrated in specific urban and northern areas. The identification of localized risk clusters extends previous exposure risk assessments [11,12] by demonstrating not only where risk levels are high, but also where high risk areas spatially cluster. Similar emphasis on spatially targeted $PM_{2.5}$ risk management has also been reported in Thailand [13].

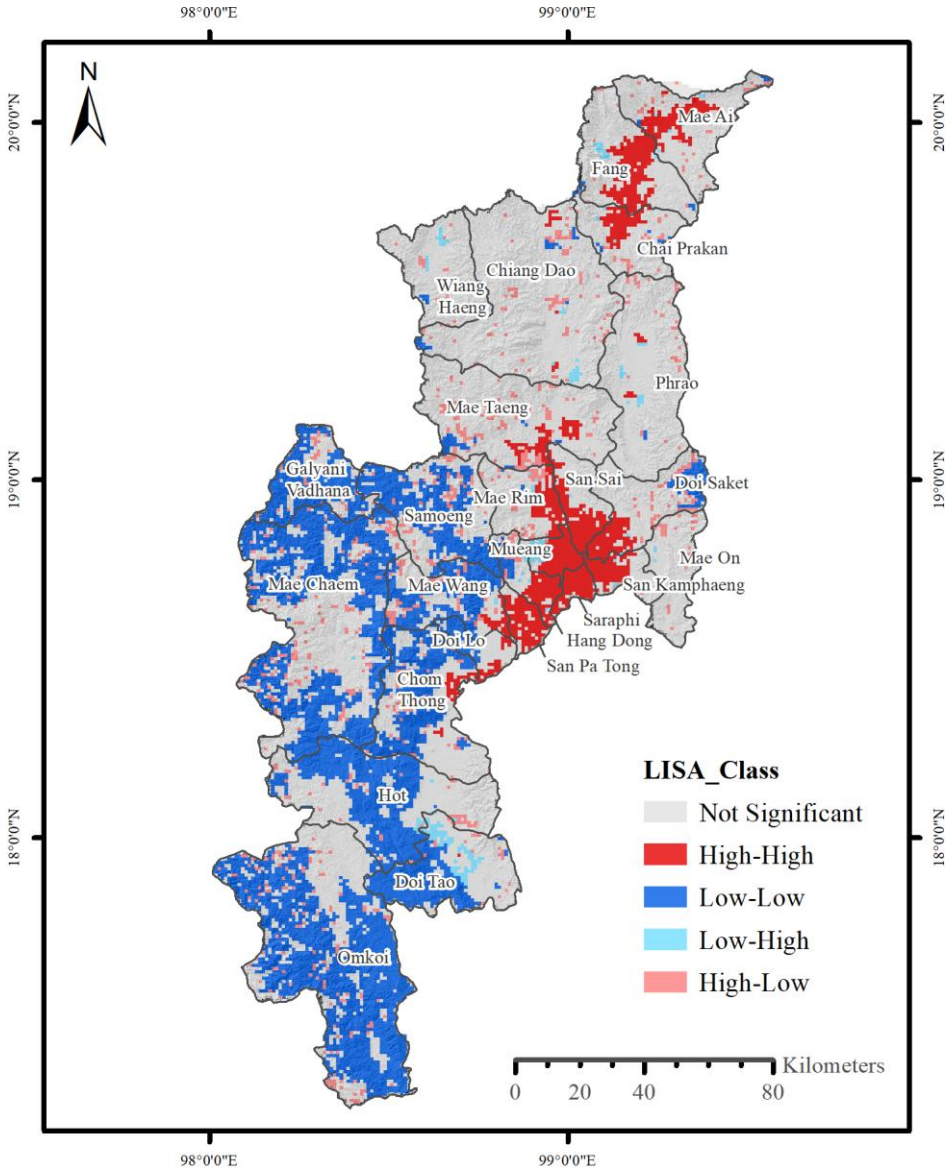

Figure 6. Spatial clusters of $PM_{2.5}$ risk in Chiang Mai Province.

3.3 Discussions

The spatial risk patterns revealed in this study emphasize the importance of considering $PM_{2.5}$ risk beyond pollutant concentration alone. The concentration of high- and very-high-risk areas in the central basin and northern districts reflects the spatial overlap of $PM_{2.5}$ hazard, population exposure, and vulnerability, while the LISA results indicate that these risks are spatially clustered rather than randomly distributed. The relevance of these identified hotspots is strongly supported by localized epidemiological evidence. For example, Chaiprakarn District, identified as a significant high-risk cluster in our spatial model, has independently been reported as an area where high $PM_{2.5}$ exposure significantly triggers acute exacerbations of chronic obstructive pulmonary disease (AECOPD) [18]. This severe health impact extends across the larger northern region; parallel studies in neighboring Lampang Province confirm that $PM_{2.5}$ concentrations above 50 μg/m³ are a significant risk factor for driving COPD exacerbations [19]. These findings are consistent with previous spatial $PM_{2.5}$ exposure assessments, which demonstrate higher risks where elevated concentrations coincide with dense populations [11,12], as well as with GIS-based risk mapping in Bangkok that emphasized the necessity of incorporating population and vulnerability factors into local risk assessments [13].

The spatial concentration of risk, especially around urban areas and educational institutions, has direct local preparedness implications. Schools located within high- and very-high-risk zones should consider establishing designated clean-air rooms, providing daily air-quality information, and strengthening local monitoring through additional $PM_{2.5}$ measurement points. Local authorities could also implement phase-specific preventive measures, including the distribution of masks, temporary restrictions on outdoor activities, and school closures when pollution conditions become severe. More broadly, strengthening local coping capacity provides a practical pathway for reducing vulnerability within the risk framework. This is particularly crucial because local authorities have limited ability to reduce background hazards or alter population distributions, and they frequently face transboundary pollution transported from outside the province or country. Furthermore, during severe haze events, spatial proximity to healthcare alone may not guarantee access, as high $PM_{2.5}$ concentrations act as a behavioral barrier that significantly deters individuals from traveling to health facilities [20]. Establishing community-based clean-air spaces and improving decentralized access to health services for vulnerable groups—such as young children, older adults, and patients with chronic conditions—could therefore reduce vulnerability at a relatively modest cost. Such measures can be developed through local government programs, empowering communities to strengthen their response capacity without relying entirely on central government resources.

Despite these insights, several limitations should be acknowledged. First, the present assessment is based on five-year average $PM_{2.5}$ conditions during the peak burning season (January–April) and therefore may not represent long-term or annual health risks. Urban populations also face substantial $PM_{2.5}$ exposure from local traffic emissions during the non-burning period; for instance, Chansuebsri et al. [5] reported that road transportation accounted for approximately 76% (27.2 μg/m³) of $PM_{2.5}$ during non-haze months in Chiang Mai. Second, the assessment of sensitive populations relied on the geographic locations of schools represented as point features, without incorporating quantitative comparisons of student capacity. Thus, the reported 80.73% represents the proportion of school locations within high- and very-high-risk zones rather than the absolute number of students exposed. Nevertheless, because this peak $PM_{2.5}$ period coincides directly with the second academic semester, ensuring that schools at all educational levels are equipped with safe learning spaces remains a critical priority to mitigate exposure risks. Finally, a methodological limitation involves the equal weighting of the two vulnerability indicators. Although this approach provides a transparent and reproducible baseline for spatial screening, it may not fully capture the relative contributions of environmental susceptibility and healthcare accessibility to overall vulnerability. Future studies should explore data-driven weighting approaches, such as the Analytic Hierarchy Process (AHP) or machine-learning methods, once appropriate local empirical data become available.

4. CONCLUSIONS

This study developed a spatial health-risk assessment framework for $PM_{2.5}$ in Chiang Mai Province by integrating satellite-derived hazard data, population exposure, and composite vulnerability indicators. The resulting assessment revealed substantial spatial heterogeneity in $PM_{2.5}$-related health risks during the peak burning season (January–April) based on conditions from 2020–2024. High- and very-high-risk zones were concentrated in the densely populated central basin, particularly in Mueang Chiang Mai, San Sai, and Saraphi districts, with a secondary concentration in the northern districts of Fang, Chai Prakan, and Mae Ai. These areas broadly overlapped with locations of elevated $PM_{2.5}$ concentrations.

Local Indicators of Spatial Association (LISA) further identified significant High–High clusters in the central basin and northern areas, while Low–Low clusters were concentrated in the sparsely populated western and southern mountainous districts, including Mae Chaem, Omkoi, and Galyani Vadhana. The northern risk clusters are also consistent with the potential influence of transboundary biomass-burning pollution near the Thai–Myanmar border reported in previous studies.

The observed spatial heterogeneity demonstrates the value of geographically targeted approaches to $PM_{2.5}$ health-risk assessment and planning. The resulting risk maps provide spatial information that can support targeted preparedness, exposure reduction, and resource allocation during the burning season. Future studies should incorporate higher-resolution temporal data, localized epidemiological information, and empirically derived vulnerability weights to improve the assessment. In addition, incorporating school enrollment and population data would allow more precise evaluation of exposure among sensitive populations.

Acknowledgement

This research was conducted as part of a Ph.D. dissertation in the Department of Geography, Faculty of Social Sciences, Chiang Mai University. Financial support for this study was provided by the Teaching Assistant and Research Assistant (TA/RA) Scholarship from Chiang Mai University. The authors thank the data providers, including NASA for the MODIS Burned Area product and Oak Ridge National Laboratory (ORNL) for spatial population data. We also thank the Google Earth Engine development team for providing cloud-computing platform that supported large-scale data processing. In addition, we gratefully acknowledge the Center for Spatial Data Science at the University of Chicago for developing the GeoDa software, which was used to conduct the spatial autocorrelation analysis. The datasets generated and analyzed during the current study are available from the corresponding author on reasonable request.

References

[1] World Health Organization. (2026). World health statistics 2026: monitoring health for the SDGs, Sustainable Development Goals. Geneva: World Health Organization.

[2] Junpen, A., Pansuk, J., Kamnoet, O., Cheewaphongphan, P., & Garivait, S. (2018). Emission of air pollutants from rice residue open burning in Thailand, 2018. Atmosphere, 9(11), 449.

[3] Suriyawong, P., Chuetor, S., Samae, H., Piriyakarnsakul, S., Amin, M., Furuuchi, M., Hata, M., Inerb, M., & Phairuang, W. (2023). Airborne particulate matter from biomass burning in Thailand: Recent issues, challenges, and options. Heliyon, 9, e14261.

[4] Suppawimut, W., & Samphutthanont, R. (2026). Deep learning-based detection of agricultural burned areas using true color satellite imagery. Geographia Technica, 21(2), 174-187.

[5] Chansuebsri, S., Kolar, P., Kraisitnitikul, P., Kantarawilawan, N., Yabueng, N., Wiriya, W., Thepnuan, D., & Chantara, S. (2024). Chemical composition and origins of PM2.5 in Chiang Mai (Thailand) by integrated source apportionment and potential source areas. Atmospheric Environment, 327, 120517.

[6] Amnuaylojaroen, T., Inkom, J., Janta, R., & Surapipith, V. (2020). Long range transport of Southeast Asian PM2.5 pollution to Northern Thailand during high biomass burning episodes. Sustainability, 12(23), 10049.

[7] Suppawimut, W., Hemwan, P., Thavorntam, W., & Charoenpanyanet, A. (2026). Spatio-Temporal Analysis of PM2.5 Concentrations through Integration of Aerosol Optical Depth and Sentinel-5P Data Using Google Earth Engine. Environment and Natural Resources Journal, 24(4), 1–15.

[8] Buya, S., Gokon, H., Huynh, V. N., Dam, H. C., Usanavasin, S., Karnjana, J., et al. (2026). Spatiotemporal association between monthly PM2.5 levels and cardiorespiratory mortality in Thailand (2015-2019). International Journal of Environmental Health Research, 36(1), 41-52.

[9] Sapbamrer, P., Assavanopakun, P., & Panumasvivat, J. (2024). Decadal trends in ambient air pollutants and their association with COPD and lung cancer in Upper Northern Thailand: 2013-2022. Toxics, 12(5), 321.

[10] Prasansri, A., Thanatrakolsri, P., & Ivanovitch, K. (2026). PM2.5 trends, mortality risks, and health benefits under air quality improvement scenarios in Northern Thailand. Atmospheric Environment: X, 31, 100490.

[11] Xu, D., Lin, W., Gao, J., Jiang, Y., Li, L., & Gao, F. (2022). PM2.5 Exposure and Health Risk Assessment Using Remote Sensing Data and GIS. *International Journal of Environmental Research and Public Health*, *19*(10), 6154. https://doi.org/10.3390/ijerph19106154

[12] Song, J., Li, C., Liu, M., Hu, Y., & Wu, W. (2022). Spatiotemporal Distribution Patterns and Exposure Risks of PM2.5 Pollution in China. Remote Sensing, 14(13), 3173. https://doi.org/10.3390/rs14133173

[13] Tabucanon, A. S., Mingkaew, J., Tiemrak, W., Moonaudom, P., & Xue, W. (2024). Application of geographic information system for PM2.5 risk assessment in Din Daeng District, Bangkok. The 5th Environment and Natural Resources International Conference (ENRIC 2024), 15-24.

[14] Pollution Control Department. (2024). Thailand air and noise pollution situation and management report, [on-line:] http://air4thai.com/tagoV2/tago_file/books/book_file/23d013df9e571981c636a8a9016d301a.pdf [access: 15.03.2026].

[15] Oak Ridge National Laboratory. (2021). LandScan Global Population Database. Oak Ridge National Laboratory. https://doi.org/10.48690/1532445

[16] Giglio, L., Justice, C., Boschetti, L., & Roy, D. (2021). MODIS/Terra+Aqua Burned Area Monthly L3 Global 500m SIN Grid V061. NASA Land Processes Distributed Active Archive Center. https://doi.org/10.5067/MODIS/MCD64A1.061

[17] Ahn, S., Oh, J., Yun, H., Min, H., Kim, Y., Kang, C., An, S., Kim, A., Kwon, D., Park, J., & Lee, W. (2025). Short-term exposure to fine particulate matter (PM2.5), cause specific-mortality, and high-risk populations: A nationwide time-stratified case-crossover study. GeoHealth, 9(10), e2024GH001214.

[18] Na Pan, T. (2023). Association between particulate matter with diameter of less than 2.5 micron with acute exacerbation of chronic obstructive pulmonary disease in Chaiprakarn District, Chiang Mai Province. Thai Journal of Ergonomics, 6(1), 1-12.

[19] Sumethvanich, P. (2023). The related between the amount of PM 2.5 and COPD exacerbation in Koh Kha Hospital, Lampang. Journal of Health Sciences Scholarship, 10(2), 31-43.

[20] Liu, Z., Liu, C., Cui, Y., et al. (2022). Air pollution and refraining from visiting health facilities: a cross-sectional study of domestic migrants in China. BMC Public Health, 22, 2007.